Marine Chemistry 254 (2023) 104277

Contents lists available at ScienceDirect

Marine Chemistry

journal homepage: www.elsevier.com/locate/marchem

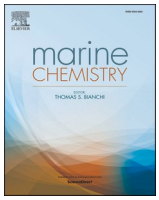

Trace metal dissolution kinetics of East Asian size-fractionated aerosols in seawater: The effect of a model siderophore

Hsin-Yen Wu [a,b], Chih-Chiang Hsieh [a,b], Tung-Yuan Ho [a,b,*]

[a] Research Center for Environmental Changes, Academia Sinica, Taipei, Taiwan
[b] Institute of Oceanography, National Taiwan University, Taipei, Taiwan

ARTICLE INFO

Keywords:
Aerosol
Trace metals
Dissolution kinetics
Anthropogenic aerosols
Lithogenic aerosols
Organic ligands
Siderophore
The East China Sea
GEOTRACES

ABSTRACT

Aerosol soluble metals are considered bioavailable to marine phytoplankton and may influence phytoplankton growth, their community structure, and material cycling in the ocean. The dissolution is controlled by the physical and chemical properties of aerosols and various atmospheric, physical, and biogeochemical processes before and after depositing in the surface water. Among these complicated processes, the interaction of aerosol metals with organic ligands in seawater is one of the major factors. In this study, we systematically investigated the dissolution kinetics of trace metals from fine (0.45–0.95 μm) and coarse (>7.2 μm) aerosols in seawater for 30 days under conditions with or without adding a model Fe organic ligand, siderophore desferrioxamine B (DFB). We found that most of the soluble metals in the fine aerosols were leached rapidly within the first hour. In terms of the coarse aerosols, with DFB addition, the fractional solubility of Fe increased substantially from 0.1 to 10%, and the solubilities of most other metals generally increased by about 2-fold within 30 days. Without DFB addition, we found that most soluble metals were still gradually released over time in coarse aerosols, except particle-reactive metals, Fe and Pb. We further observed strong linear correlations between dissolved metals (Al, Fe, Mn, Co, Ni, and Zn) and silicate concentrations for DFB addition with coarse aerosols, with metal to silicate ratios comparable to those of typical aluminosilicates. Quantitatively, the aluminosilicate-associated dissolved metals accounted for >85% of total dissolved Fe, Al, and Co, and 40–60% for total dissolved Mn and Ni with the addition of DFB for 30 days. By comparing dissolved metal to Al ratios with lithogenic ratios, the metals leached in the first hour for both coarse and fine aerosols originated from anthropogenic sources, and lithogenic aerosols gradually became the dominant soluble metal source for coarse aerosols after 1 h, extending to 720 h. The findings of this study exhibit the importance of the time-dependent interaction of lithogenic aerosols with organic ligands in seawater. The residence time of aerosol particles and the concentrations of available organic ligands in the euphotic zone are key factors affecting aerosol dissolved metal availability to marine phytoplankton in the surface ocean.

1. Introduction

Aerosol deposition is a major external source of trace metals in the surface ocean (Duce et al., 1991; Jickells et al., 2005; Mahowald et al., 2018). Aerosol dissolved metals, such as Fe, Mn, Zn, Cu, Co, Ni, and Cd, may thus influence the growth and community structure of phytoplankton and material cycling in the ocean (Morel and Price, 2003; Saito and Goepfert, 2008). Since soluble metals are generally considered bioavailable for marine phytoplankton (Morel, 2008), quantifying the contribution of aeolian soluble metals in the euphotic zone is essential to evaluate the biogeochemical impacts of aerosol input in the ocean. The physical and chemical properties of aerosols, including the sources, compositions, sizes, and metal speciation, are all critical factors in affecting the dissolution of aerosol metals. In terms of the sources, mineral dusts are one of two major components, particularly for oceanic regions located downwind of desert areas, such as the North Atlantic Ocean for the Sahara and the Northwestern Pacific Ocean from the Gobi Desert. On the other hand, anthropogenic aerosols can also be a significant source and are generally composed of fine particles with highly soluble trace metals. Anthropogenic aerosols are particularly important in the oceanic regions located downwind of large population regions, such as East and South Asia (Hsieh et al., 2022). The relative

* Corresponding author at: 128, Sec. 2, Academia Rd., Nankang, Taipei 115, Taiwan.
E-mail address: tyho@gate.sinica.edu.tw (T.-Y. Ho).

https://doi.org/10.1016/j.marchem.2023.104277
Received 17 January 2023; Received in revised form 30 June 2023; Accepted 2 July 2023
Available online 7 July 2023

contribution of soluble trace metals from lithogenic and anthropogenic aerosols to the global ocean still largely remains unclear. In addition, aerosol size can reflect aerosol sources and may be strongly associated with the solubilities of aerosol metals in seawater. Using size-fractionated aerosol samples collected over the East China sea, Hsieh et al. (2022, 2023) have shown increasing solubilities of Fe and all other trace metals with decreasing aerosol sizes, which linearly correlated with the non-sea-salt sulfur. Size-fractionated aerosol sampling can thus facilitate the investigation of the relative contribution of soluble trace metals from lithogenic and anthropogenic aerosols.

In surface waters, dissolved trace metals are largely complexed by organic ligands (Bruland et al., 2013; Ellwood and van den Berg, 2001). Indeed, the dissolved concentrations of many trace metals in seawater are decided by the availability of organic ligands. Using aerosol Fe as an example, without complexation by organic ligands, aerosol soluble Fe would precipitate and be scavenged quickly due to its extremely low solubility in high pH seawater and its high particle reactivity. Moreover, extended leaching experiments with seawater have shown that strong Fe-binding ligands (e.g., siderophore) promotes Fe dissolution from Fe (III) bearing minerals, aerosols, and lithogenic particles (Borer et al., 2005; Fishwick et al., 2014; Kessler et al., 2020). Siderophores are low-molecular-weight Fe-chelating organic ligands with high affinity for Fe (III) and have been extensively used to study ligand-promoted dissolution of Fe-containing minerals. Studies have investigated their distribution extensively and discovered their universal presence in all studied regions (Boiteau et al., 2016; Moore et al., 2021). For instance, the concentrations of ferrioxamine siderophore ranged from 0.1 to 2 pM in the surface ocean at the ALOHA station (Bundy et al., 2018) and ranged from 4 to 14 pM in the surface ocean of the North Pacific Ocean (Park et al., 2022). In addition to complexing Fe, DFB may complex other trace metals. Actually, the conditional stability constants of DFB with divalent Cu, Zn, and Pb are comparable with those of their element-specific organic ligands in natural seawater (Schijf et al., 2015), suggesting that the dominant ligands for these metals are siderophore-like. For example, siderophores have exceptionally high complexation constants for trivalent Co (and Mn); five orders of magnitude higher than that of Fe (III) (Duckworth et al., 2009). Siderophores may thus promote the dissolution of cobalt oxyhydroxides (Bi et al., 2010; Akafia et al., 2014). In brief, siderophores are ideal model organic ligands to study aerosol trace element solubility in laboratory. Studies of the influences of organic ligands on aerosol trace metal dissolution (other than Fe) in seawater are extremely limited. This study reports how DFB influences the dissolution of a suite of aerosol trace metals with time in seawater.

The residence time of aerosols in the euphotic zone is a major factor influencing the dissolution aerosol metals. A few studies have reported the residence time of total (dissolved and particulate) or particulate metals in surface waters of the open ocean where aerosol input was likely to be the dominant metal source. Croot et al. (2004) reported that the residence time of total Fe was 6–62 days in the surface water of the equatorial Atlantic Ocean. The residence time of particulate Al and Ti were 3–22 and 4–37 days, respectively, in the surface water of the tropical and subtropical North Atlantic (Dammshäuser et al., 2013). Compiling global ^{234}Th and sediment trap data, Black et al. (2020) suggested that the residence time of lithogenic particulate Fe ranged between 10 and 100 days in the global surface ocean. Atmospheric input has been identified to be the major source of most particulate trace metals in the surface water of the South China Sea (Ho et al., 2007, 2010b, 2011). Using floating trap and aerosol sampling, the estimated residence times of particle-reactive metals, including Fe, Al, Ti, Pb, and Th, ranged from 10 to 20 days in the surface layer; and the residence times of Mn, Zn, Co, Ni, and Cd were 50, 62, 292, 361, and 3650 days, respectively (Ho et al., 2007; 2009; Ho et al., 2010b; Ho et al., 2011). Based on the information obtained in these field studies, a reasonably long leaching time in laboratory studies is needed to mimic the dissolution kinetics of aerosol metals in nature. We thus decided to carry out a 30-day long aerosol leaching experiment.

Adjacent to East Asia, the East China Sea receives high fluxes of both fine anthropogenic and coarse lithogenic aerosols, serving as an ideal sampling location to collect aerosol samples for solubility experiments. We have used the size-fractionated aerosols collected in an islet located in the East China Sea, Matsu, which is close to mainland China, to investigate the interactive effects of aerosol sizes and DFB on the dissolution kinetics of eight aerosol trace metals in seawater. We have chosen two extreme size fractions of aerosols for this study, the finest (0.45–0.95 μm) and coarsest (>7.2 μm) aerosols and conducted a 30-day time-series dissolution experiment with DFB. We first examined the trace element ratios and dissolution fractions and characterized their dissolution kinetics and discussed the potential causes. We also investigated how DFB affects the dissolution kinetics of aerosol metals and have further identified the sources extracted by DFB by using dissolved metal to silicate ratios. The findings of this study shall provide insights into the quantitative estimate of aerosol dissolvable metals in the surface ocean.

2. Methods

2.1. Size-fractionated aerosol sampling

Matsu islet is located in the East China Sea (26.17°N; 119.92°E), only 19 km away from mainland China (Fig. 1). The sampling station is established on the roof of a two-story building, with a height about 6 m above the ground. Size-fractionated aerosols samples were collected on polytetrafluoroethylene (PTFE) filters (TE-230-PTFE, Tish Environment Inc., US) using a high-volume air sampler (TISCH Environmental Inc., US, MODEL-TE-5170) with a cascade impactor (TISCH Environmental Inc., US, Series 235). The aerosol samples were collected for a week continuously in December 2020 when the prevalent northeastern monsoon transported high fluxes of East Asian aerosols to adjacent ocean regions. The cascade impactor divides aerosol samples into five size fractions, including: >7.2 (abbreviated as f5), 3.0–7.2, 1.5–3.0, 0.95–1.5, and 0.45–0.95 μm (f1). We chose the finest and largest fractions, labelled as f1 and f5, to carry out the leaching experiments in this study (Fig. 1). For each size fraction, aerosol samples were collected and distributed over ten strips of the filter substrate. Due to the possible uneven distribution of aerosols across all strips (Fig. 1), we have used the software ImageJ to quantify the density of the grayscale on high-resolution images of each strip. Using the software to compare the grayscale density of different strips to the strip on which we actually measured the concentrations, we may quantify the total aerosol masses on each one.

2.2. Dissolution experiments with time

Aerosol dissolution experiments were performed in natural surface seawater for 30 days to investigate the dissolution kinetics of aerosol metals and the effects of DFB addition. Seawater was collected on a research cruise in 2018 in the Western Philippine Sea (21.90°N; 123.19°E) and was immediately filtered on board using acid-washed 0.22 mm Polycap capsule filters (Whatman). The seawater was stored in a polyethylene carboy and covered with black polyethylene plastic bag at room temperature for storage. The background concentrations of dissolved trace metals and silicate were determined right before the experiments (Ho et al., 2010a; Wang et al., 2014). The concentrations of trace metals in the seawater are comparable to the concentrations observed at a close by station from our 2014 GEOTRACES Taiwan Cruise (Table S1). DFB was freshly prepared by dissolving desferrioxamine B mesylate salt (Sigma-Aldrich, > 92.5%) in Ultrapure water (Milli-Q, Millipore) before dissolution experiments. The concentration of DFB added was based on information from previous studies in the surface water of the Northwestern Pacific Ocean (NWPO), including the aerosol Fe fluxes, the concentrations of particulate Fe in suspended particles, and the concentration levels of strong Fe-binding ligands obtained. We

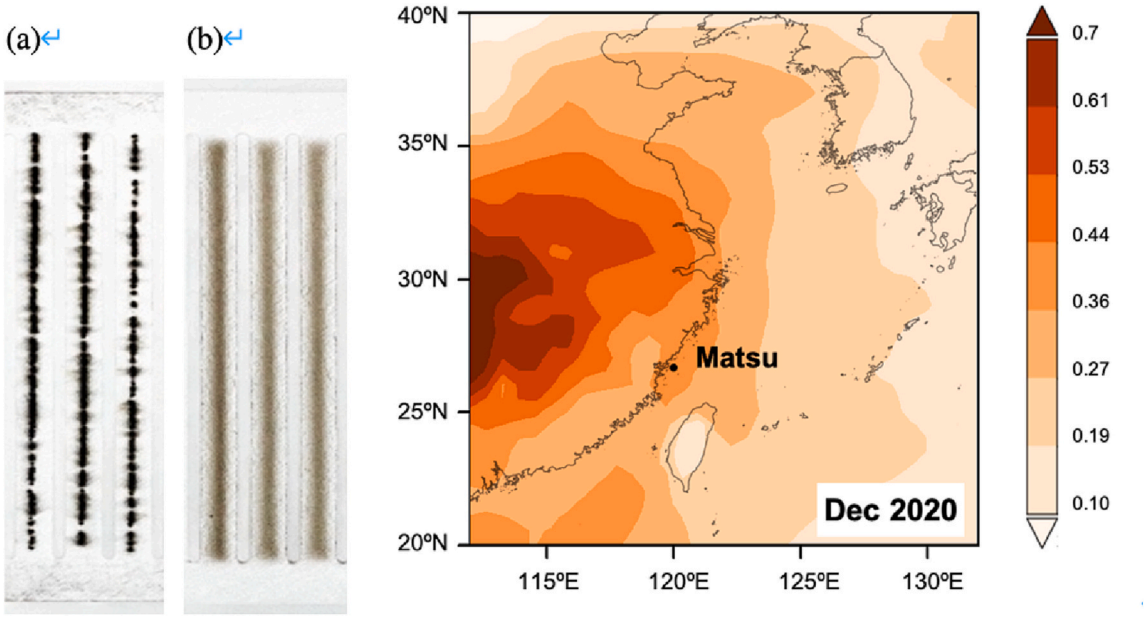

Fig. 1. (Left panel) The size-fractionated aerosols samples (a) f1 (0.45–0.95 μm) (b) f5 (> 7.2 μm). (Right panel) The location of the sampling station, Matsu islet, and the monthly averaged aerosol optical depth during the sampling period in December 2020. The aerosol optical depth was obtained from NASA Giovanni. (https://giovanni.gsfc.nasa.gov/giovanni/).

have calculated the total aerosol Fe fluxes during high flux seasons based on the data of Wang and Ho (2020), which reported about 1 nM increase of total Fe concentration in the surface 10 m seawater. The concentration levels of the strong Fe-binding ligands ranged from 1 to 2 nM and the suspended particulate Fe ranged from 1 to 3 nM, respectively (Kondo et al., 2021; Wang and Ho, 2020). We set the ratio of the concentrations of DFB to total Fe as 2:1 in our dissolution experiment. To be able to accurately detect the soluble concentrations of trace metals in this experiment, aerosol loadings and DFB concentrations applied are much higher than natural conditions, with DFB final concentrations to be 4 and 15 μM for f1 and f5 samples. Thus, it should be noted that these experimental conditions do not replicate the real ocean.

Dissolution experiments were conducted with and without the addition of DFB, referred to as Control and DFB treatments hereafter (Fig. 2). All chemical reagents used in this study were ultrapure grade, including hydrochloric acid, nitric acid, and hydrofluoric acid (J.T.

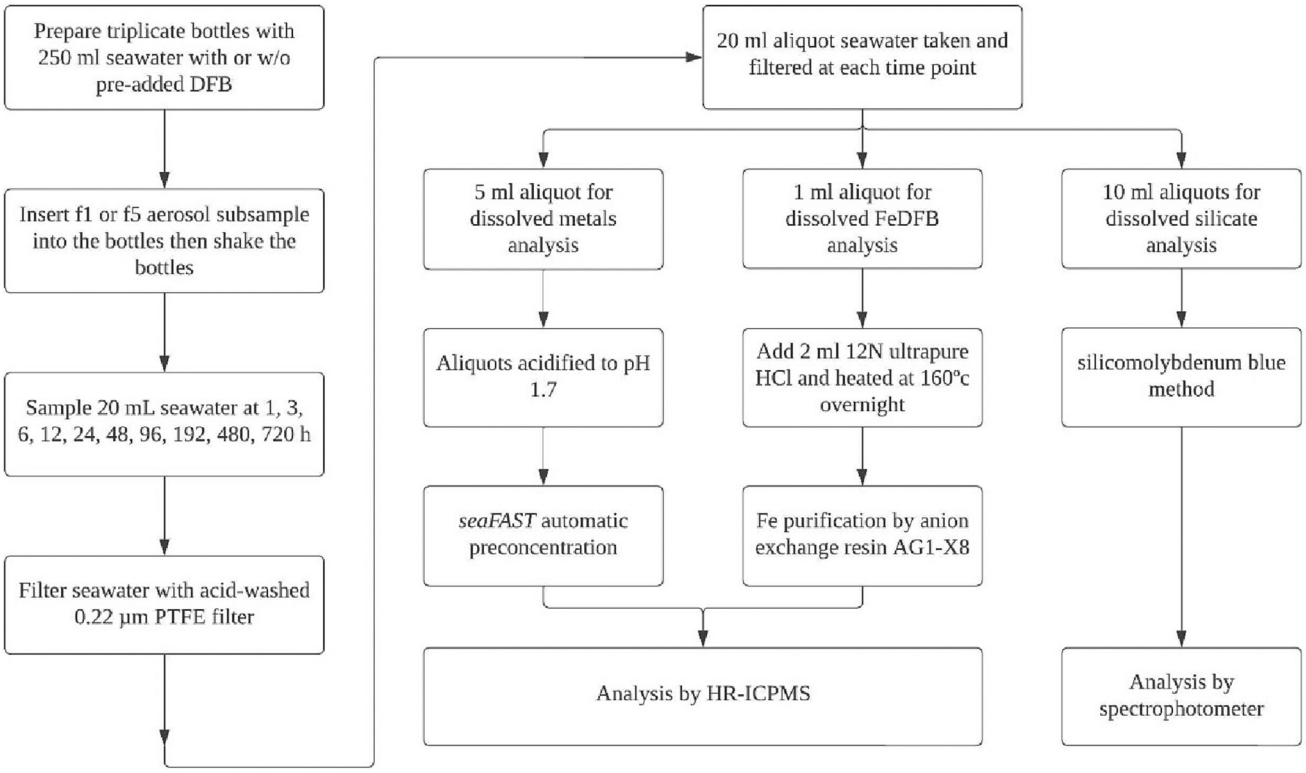

Fig. 2. A flow diagram showing the procedures of the leaching experiments of this study. The detailed procedures are also described in the Methods section.

Baker). All the experiments were carried out in a positive pressured class 5 cleanroom, either in a HEPA-filtered class 5 laminar flow bench or hood. For DFB treatment, DFB was pre-added into seawater before adding aerosol samples and carrying out the batch leach experiments (Fig. 2). All experiments were carried out in three replicate bottles ($n = 3$). The whole strips of aerosol sub-samples were inserted into triplicate acid-washed low-density polyethylene bottles with 250 mL seawater and placed on an orbital shaker (Firstek, Model-S101), which was set to rotate at 120 rpm to mimic natural conditions. Aliquots (20 mL) were taken out from each replicate bottle at 1, 3, 6, 12, 24, 48, 96, 192, 480, and 720 h during the experimental period. The soluble metals at the first time point, 1 h, is operationally defined as the instantaneously soluble fraction in this study. During the 720 h sampling period, we have cautiously taken samples to maintain the concentrations of the aerosol particles in the bottles to be homogenous as much as possible. Through our preliminary test, we found that the colour of the aerosol filter strips were significantly faded after 1 h shaking, showing that most of the aerosols were detached from the filters in 1 h. Before taking the 20 mL aliquots each time, the bottles were well mixed to maintain the suspended aerosol particles to be homogenous in the bottle even though we did not observe any sinking particles at the bottom of the bottles. Indeed, the contrasting but systematic patterns for the solubility of some elements (e.g., Fe vs Pb) observed for Control treatments support that the aerosol concentrations were relatively stable during the sampling period. Once sampled, aliquots were then filtered through 0.22 μm pore size 13 mm diameter PTFE syringe filters (Advantech) into acid-washed 50 mL PP tubes and 15 mL PP tubes for the measurement of dissolved trace metals and silicate concentrations. The aliquots for dissolved metal samples were acidified with HCl (ultrapure, J. T. Baker Inc.) immediately after sampling to reach the final H^+ concentration of 0.020 N or at pH 1.7.

2.3. Quantification of dissolved metal concentrations and fractional solubility

Total aerosol metal concentrations were obtained by digesting separate aerosol sample strips in a freshly prepared mixture of 4 M HF, 4 M HCl, and 4 M HNO_3 on a hotplate for 4 h at 120 °C (Ohnemus et al., 2014). After drying at 120 °C 4 mL 0.5 N HNO_3 was added and digested at 120 °C again for 1 h. One 0.1 mL aliquot of the digested samples were then diluted 100 times with 0.5 N HNO_3 with 1 ppb of indium as an internal standard before ICPMS analysis. The control seawater samples for aerosol dissolved trace metal analysis (no DFB added) were all processed using a sea*FAST* automated preconcentration system (Elemental Scientific) to remove major salts and preconcentrate trace metals. The metal concentrations were then quantified using a HR-ICP-MS (Element XR, Thermo Scientific) fitted with a desolvation system (Omega HF, Elemental Scientific). The detailed information on the analytical method, blank, precision, and accuracy were reported in our previous studies (Ho et al., 2010a; Wang et al., 2014). In brief, the isotopes of ^{115}In, ^{111}Cd, ^{114}Cd, ^{207}Pb, and ^{208}Pb were determined at low resolution ($M/\triangle M \sim 300$), while ^{27}Al, ^{47}Ti, ^{49}Ti, ^{51}V, ^{55}Mn, ^{54}Fe, ^{56}Fe, ^{59}Co, ^{58}Ni, ^{60}Ni, ^{61}Ni, ^{64}Zn, ^{66}Zn and ^{115}In were analyzed at medium resolution ($M/\triangle M \sim 4000$). We used NIES CRM No. 28 Urban Aerosols collected in Beijing (National Institute for Environmental Studies), NASS-7, and CASS-6 (National Research Council Canada) as reference materials to validate the accuracy of the analysis for both aerosol and seawater samples, respectively. The ratios of our measured value to the certified value for reference materials are presented in Table S2. Fractional solubilities of each trace metal were calculated by dividing the dissolved metal concentrations measured in 0.22 μm filtered seawater samples by the total aerosol metal concentrations.

2.4. Quantification of Fe-DFB complexes in seawater

The measurement of Fe-DFB concentrations in seawater is challenging due to its strong conditional stability constants with Fe. The typical analytical methods for dissolved Fe concentrations in seawater generally use chelating resins to complex Fe from pH buffered samples while simultaneously washing out major ions to remove the seawater matrix for further analysis by ICPMS. The chelating resin used in the sea*FAST* preconcentration system, Nobias PA-1, effectively binds transition metals under a pH range of 5–7 (Sohrin et al., 2008). However, we found that the Nobias PA-1 resin in a *seaFast* system does not extract Fe from Fe-DFB complexes in the experiments where the DFB concentrations were 1 μM (Table S3). To extract Fe from Fe-DFB in seawater, we have modified the typical column chemistry purification method used in trace metal isotope analysis (Dauphas et al., 2004). The Fe-DFB samples were amended to 8 N HCl and passed through anion-exchange columns loaded with AG1-X8 (Bio-Rad) (Dauphas et al., 2004). Acidification to 8 N HCl facilitates the dissociation of DFB-Fe complexes and allows anionic Fe chloride complexes to be adsorbed on AG1-X8. Using different eluting acids with different H^+ concentrations, we can separate Fe from other major cations. In detail, 1 mL seawater samples from dissolution experiments containing Fe-DFB complexes were mixed with 2 mL 12 N HCl and heated on a hotplate at 160 °C overnight. One mL AG1-X8 resin was loaded into the purification column and cleaned by passing 10 mL of 2 N HNO_3 and 3 mL of MQ water. After conditioning the resin using 3 mL of 8 N HCl, the seawater samples were loaded onto the column and allowed to pass through by gravity at flow rate of 0.3 mL per minute. The major ions in seawater were removed using 3 mL of 8 N HCl then the Fe fraction was collected using 2 mL of 0.5 N HNO_3. The average Fe recovery of the eluted samples were higher than 98% (Table S3). Procedural blanks were determined by using MQ water without Fe addition as samples. The Fe recovery of Fe-DFB in seawater is obtained by dividing the concentrations of Fe-DFB to the concentrations without DFB addition, which was determined in acidified seawater processed using the *seaFAST* preconcentration system (Table S3).

2.5. Silicate measurements

The measurement of dissolved silicate followed the silicomolybdenum blue method (Ramachandran and Gupta, 1985). Briefly, 0.22 μm filtered seawater samples were added with the mixed reagents of sulfuric acid and ammonium molybdate. The second mixed reagents of citric acid and potassium antimony tartrate trihydrate and the third reagent ascorbic acid were subsequently added. The absorbance was then determined using a 10 cm path length cell on a spectrophotometer (Shimadzu Corp., Model-UV-1700) at 810 nm.

3. Result and discussion

3.1. Enrichment factors, trace metal solubility, and aerosol sources

Enrichment factors (EF hereafter) of aerosol metals can be a complementary parameter to evaluate the contribution of anthropogenic aerosols for some elements. The EF of aerosol metals are generally calculated from the ratios of metal to Ti (or Al) in aerosol samples divided by the ratio in the upper continental crust (UCC) (Hu and Gao, 2008).

$$EF = (Metal/Ti)_{aerosol}/(Metal/Ti)_{UCC}$$

It is known that metals in anthropogenic aerosols are often highly enriched in comparison with their natural abundance in lithogenic aerosols. For f1, the EF values for the elements Cd, Zn, Pb, Ni, Mn, Co, Fe, and Al were 9929, 799, 765, 127, 43, 12, 4.9, and 1.1, respectively; for f5, the EF values for the same elements were 59, 30, 11, 20, 4.9, 4.3, 2.9, and 1.4 (Fig. 3; Table S4). As the deviation of metal ratios in various UCC are generally within a factor of 3 or less (Hu and Gao, 2008), the elements with extremely high EF values in f1, such as Cd, Zn, and Pb, indicate a very significant contribution from anthropogenic aerosols. On

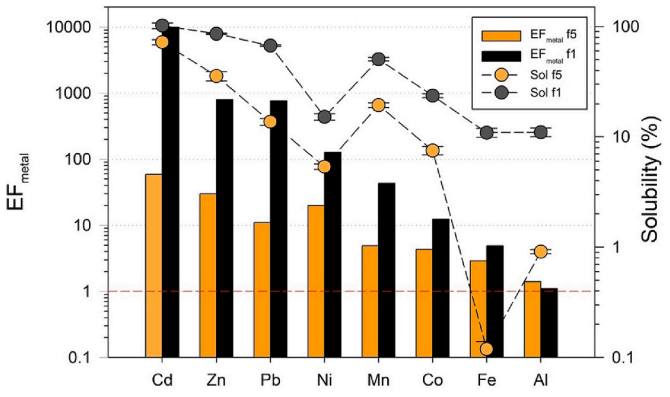

Fig. 3. The comparison of the enrichment factors (EF) and the 1 h fractional solubilities of aerosol metals in f1 and f5. The orange and black bars stand for the EF of f5 and f1, respectively. The orange and grey circles stand for the average 1 h fractional metal solubilities for f5 and f1. The EF were calculated by dividing the metal to Ti molar ratios in aerosol samples ($n = 1$) by the ratios in upper continental crust (Hu and Gao, 2008). The average fractional metal solubilities are shown as the mean of three replicate bottles ($n = 3$).

the other hand, elements with EF values close to 1 are generally considered to originate from a lithogenic source. However, it should be noted that some metals (e.g., Al and Fe) in anthropogenic aerosols may possess similar metal to Ti ratios as the ratios in lithogenic sources (Hsieh et al., 2023). Although the EF of Fe (or Al) in fine aerosols are close to 1 or 2, the solubilities can be two orders of magnitude higher than coarse aerosols. The slight increase of the EF of Fe with decreasing aerosol sizes suggests that the highly soluble Fe originated from anthropogenic aerosols (Hsieh et al., 2023).

Fig. 3 compares the EF values with the solubilities of metals in aerosol samples dissolved within the first 1 h of the dissolution experiment of this study. For Cd, Zn, Pb, Ni, Mn, and Co, the consistency of higher EF and solubilities of f1 than f5 supports that anthropogenic aerosols are the dominant source for f1 (Fig. 3). For Al and Fe, although their EF are close to 1 and comparable between f1 and f5, the solubilities of f1 are 10-fold and 100-fold of those of f5, respectively, indicating that anthropogenic aerosols were the dominant source for soluble Al and Fe in f1 as the study of Hsieh et al. (2023) has shown.

3.2. The dissolution kinetics of aerosol metals without DFB addition

Figs. 4 shows the dissolution kinetics of aerosols metals obtained in this study. By investigating the dissolution behavior of aerosol metals in seawater over 7 days, Mackey et al. (2014) categorized the dissolution

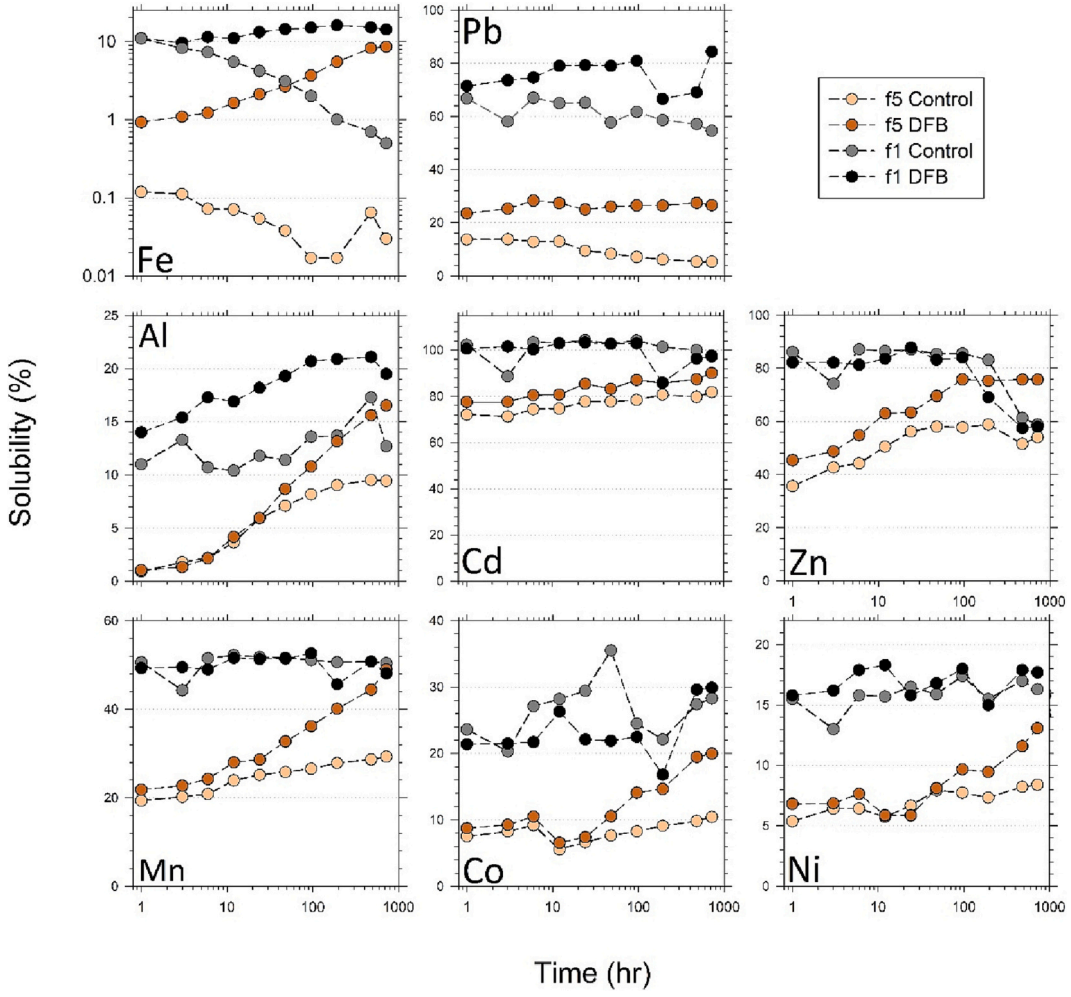

Fig. 4. The dissolution kinetics of aerosol trace metals for f5 and f1 in Control and DFB added treatments. The symbols of light orange, brown, grey, and black stand for the fractional solubilities of Control and DFB treatment for f5 and f1, respectively. The averaged solubilities of all metals are obtained from the mean of three replicates. The standard deviation (± SD) are shown in Table S5 and S6. (For interpretation of the references to colour in this figure legend, the reader is referred to the web version of this article.)

patterns of the elements into three types: particle-reactive, gradual, and rapid dissolution. In that research. Particle-reactive metals like Fe and Pb generally exhibited decreasing solubilities over time, whereas Al, Mn, and Ni displayed gradually increasing dissolution. For Cd and Co, the majority of dissolved metals were leached immediately (Mackey et al., 2014). In our study, for the Control leaching experiments using f1 aerosols, most metals, except Fe and Pb, did exhibit a rapid dissolution pattern, with metals leached instantly (Fig. 4). The solubilities for the Control f1 samples from 0 to 720 h were 11 to 0.5% (Fe), 11 to 13% (Al), 102 to 98% (Cd), 67 to 52% (Pb), 66 to 59% (Zn), 51 to 50% (Mn), 24 to 28% (Co) and 15 to 14% (Ni) (Table S5). Since the solubilities of many metals during 0–1 h have already or almost reached the maximum value, the dissolution rates were highest during the initial period (Figs. 4 and 5). The dissolution rates of later periods are thus extremely low or even negative due to precipitation and adsorption effects (Fe and Pb) or undetectable variations with time (Fig. 5).

The rapid dissolution observed for the metals in the Control f1 samples may be explained by the presence of highly soluble compounds. Using Pb as an example, Sakata et al. (2014, 2017) have identified $PbSO_4$ and $2PbCO_3{\cdot}Pb(OH)_2$ as the dominant species in fine and coarse aerosols respectively. They also reported that both PbC_2O_4 and $Pb(NO_3)_2$ were common species in both fine and coarse aerosols. The relatively high solubility of the Control f1 aerosols in our study may be due to the relatively high content of $PbSO_4$ and $Pb(NO_3)_2$. Other non-crystalline matrices in anthropogenic aerosols that weakly bind metals may also contribute to the rapid dissolution of metals, such as carbonaceous compounds, a major matrix in fly ash from heavy oil combustion (Desboeufs et al., 2005).

Reactions with strong inorganic acids and their precursors, e.g., SO_X and NO_X, are an important process to promote the dissolution of aerosol metals. Baker et al. (2020) have suggested that the elevated Fe, Al, and Ti solubilities observed in their fine aerosols may be attributed to the acid processing of non-sea-salt (nss-) sulfate. Hsieh et al. (2022) observed a linear relationship between Fe solubilities with nss-sulfur using size-fractionated aerosols that were also collected at Matsu. In addition, using synchrotron-based X-ray absorption spectroscopy, some studies show that metal sulfates are the dominant species for Fe, Ni, and Zn in fine aerosols from combustion sources (Osán et al., 2010; Huggins et al., 2011; Pattanaik et al., 2012). For Mn, Mn sulfate could also be one of the dominant species in fine aerosols collected in urban areas, in addition to other Mn species such as Mn acetate and Mn chloride (Datta et al., 2012). Baker et al. (2020) have also shown elevated Co solubility with decreasing size that correlated with higher nss-sulfate in one of their sampling stations where mineral dust was a relatively minor source.

For f5 Control samples, most metals, including Al, Cd, Zn, Mn, Co, and Ni, generally exhibited a gradual dissolution pattern with time and the solubilities of Fe and Pb exhibited particle-reactive dissolution (Fig. 4). The solubility of Zn reached its maxima at 48 h and started decreasing after 192 h. The variations of the solubilities from 0 to 720 h were 0.12 to 0.017% (Fe), 0.91 to 9.4% (Al), 0.11 to 0.99% (Si), 71 to 81% (Cd), 14 to 5.3% (Pb), 27 to 45% (Zn), 19 to 29% (Mn), 7.5 to 10% (Co) and 5.3 to 8.4% (Ni) (Fig. 4; Table S6). Similar to f1, the dissolution rates for f5 were also highest during 0–1 h (Fig. 5). Unlike f1, the solubilities of most metals in f5 were relatively low at the initial time point, so that the increases in solubilities with time were clearly observed, exhibiting a gradually decreasing dissolution rate with time. With different reactivities and thermodynamic stabilities in seawater, various metal compounds in lithogenic aerosols would possess different solubilities and equilibrium times in seawater. The initial high dissolution rates in our study were likely attributed to the most soluble non-lithogenic components in aerosols, such as salts, amorphous, or poorly crystallized minerals. The relatively low dissolution rates during 1–720 h could be attributed to high percentage of metals bound by strong

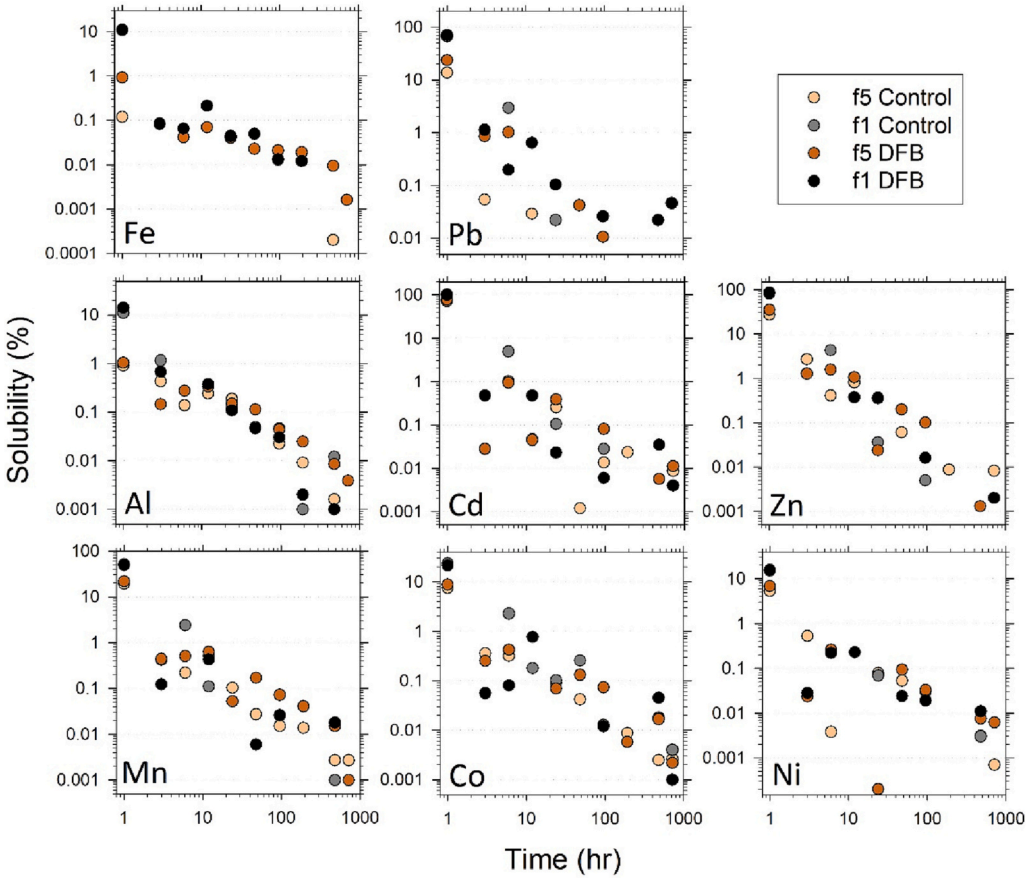

Fig. 5. The dissolution rates of aerosol trace metals of f5 and f1 in Control and DFB treatments. The symbols of light orange, brown, grey, and black stand for the dissolution rates of Control and DFB treatment for f5 and f1, respectively. The dissolution rates (% h^{-1}) are calculated with the fractional solubility difference between one sampling time point and its previous one, including the intervals 0–1, 1–3, 3–6, 6–12, 12–24, 24–48, 48–96, 96–192, 192–480, and 480–720 h. Only positive values are plotted. (For interpretation of the references to colour in this figure legend, the reader is referred to the web version of this article.)

covalent bonds in the crystalline lattice of different types of lithogenic minerals. Similar dissolution kinetics of lithogenic particles have been reported in previous studies (Desboeufs et al., 1999; Thuróczy et al., 2010). For instance, Fe can be in strong Fe—O lattice bonds as Fe(hydr) oxides or substitute Al or Si in the crystalline structure of aluminosilicates. The dissolution of these strongly bound metals would thus be a relatively slow and time-dependent process, either through the hydrolysis by hydroxide ions or complexation by organic ligands. The residence time of aerosol particulate metals in the euphotic zone would be critical for deciding their final metal solubilities and amount in the surface water of the ocean.

3.3. DFB addition retains and promotes the dissolution

Fig. 4 shows that DFB addition either retained or significantly promoted the dissolution of aerosol metals in seawater over time, particularly for f5. For Fe, the solubility of f5 increased from 1 to 9% with DFB addition in comparison to the decreasing solubility from 0.1 to 0.03% for non-DFB Control over 720 h. For f1, the solubilities at the initial period (1 h) for treatments with and without DFB addition were identical, which were both about 10%. For DFB addition treatment, the solubility was slightly increased to 16% over 720 h, but the solubility decreased from 10 to 0.4% for non-DFB addition over time (Fig. 4). Similar effects of solubility enhancement were observed for Pb and Al with DFB addition for both f1 and f5 in comparison to non-DFB addition treatments (Fig. 4). For Al, the enhancement for f5 became obvious after 24 h. Using aerosol samples collected from Penjiayu islet in the East China Sea, similar solubility enhancement features were observed for Fe, Al, Ti, and Pb (Hsieh et al., 2023). Using buffer leaching treatment (soaked in 1.4 M of ammonium acetate (pH 4.7) at room temperature for 1 h on f5, solubilities increased about one order of magnitude for Fe, Al, Ti, and Pb, while the effect on f1 was negligible (Hsieh et al., 2023). In terms of Cd, DFB addition showed little effect on its solubility for both f5 and f1 over 720 h. For Zn, Mn, Co, and Ni, the addition of DFB had an insignificant effect on their solubility for f1, except for some intermediate time points for Co. However, for f5, the solubility generally increased by around 1.5 to 2-fold from 24 to 720 h (Fig. 4). Although the initial Fe dissolution rates ($0-1h$) with DFB addition were one order of magnitude higher for f1 (10% h^{-1}) compared to f5 (1% h^{-1}), the rates during 1–192 h exhibited comparable values for both f1 and f5, decreasing from 0.1 to 0.01% h^{-1} (Fig. 5). This suggests that f1 and f5 may have similar sources of DFB-extractable Fe. The dissolution rate patterns of Al, Mn, Zn, Co, and Ni in f5 with DFB addition were similar to those without addition, showing a gradually decreasing trend over time but with enhanced rates after 24 h (Fig. 5). For f1, the dissolution rates of these metals after 1 h with DFB addition were indistinguishable from those without addition.

Clay minerals are a major component of Asian dust, accounting for over 40% of the total aerosol mass (Shao et al., 2007; Jeong, 2008; Jeong and Achterberg, 2014). Assuming that clay minerals are a major source of extractable metals in f5, we investigated the correlation between DFB-extractable metals and dissolved silicate (hereafter Si) and compared metal-to-Si ratios to those of typical clay minerals (Fig. 6). Since DFB concentrations were sufficient in our leaching experiments, we assume that the high complexing capacity of DFB on aerosol particle surface would result in extracted trace metals following their original composition (M/Si ratios) in minerals, without significant effects from redox chemistry and ligand complexation between metals. A recent study

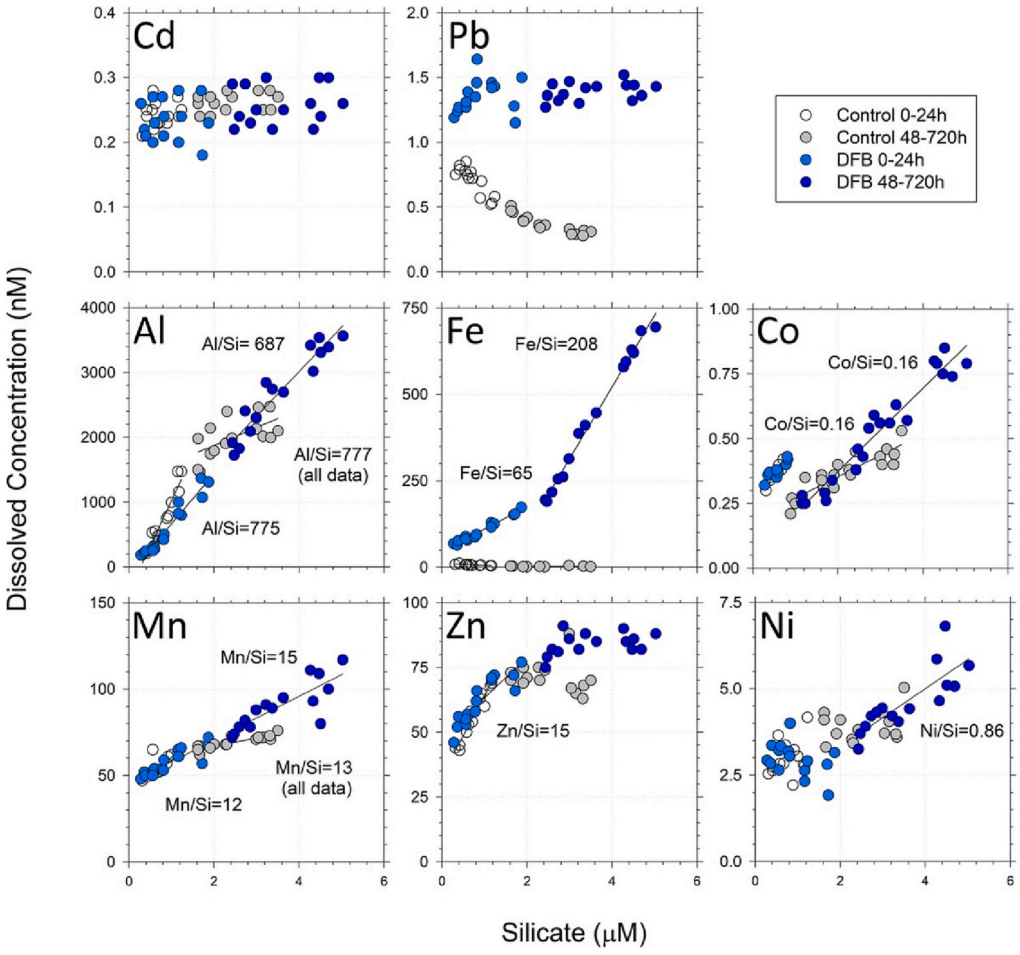

Fig. 6. The correlation of dissolved metal and silicate concentrations observed for f5 during different time intervals for both Control and DFB treatments. The data include all three replicates at all time points. The symbols of white, grey, light blue, and dark blue circles stand for the data during the intervals of 0–24 h and 48–720 h periods, respectively. For Co, the two periods are 0–6 h and 12–720 h. The metal-to-silicate slopes (mmol mol^{-1}) are only shown for highly linear segments between metals and silicate ($p < 0.001$) in DFB treatment. (For interpretation of the references to colour in this figure legend, the reader is referred to the web version of this article.)

reported that anthropogenic emissions can be a significant silicate source in the ECS (Wang et al., 2023). Assuming that the 1 h dissolvable silicate originated from anthropogenic emission (≅ 0.4 μM), Si from anthropogenic emission may account for only about 3–6% of the silicate from lithogenic aerosols which was estimated using the Al/Si slope and total Al (Fig. 6). We found significant linear correlations between Si and some DFB-extractable metals during one or two dissolution periods (Fig. 6). For Al, DFB addition significantly promoted the dissolution after 24 h, with a slope of 687 mmol Al mol^{-1} Si ($r^2 = 0.91$), comparable to the reported bulk ratios of several clay minerals in Asian dust samples. The ratios are 675 and 622 mmol Al mol^{-1} Si for illite and chlorite, respectively (Table S8). Fe also exhibited two-stage linear correlations with Si for the DFB addition treatment, during 0–24 and 24–720 h periods (r^2 = 0.97 and 0.99), with slopes of 65 and 208, respectively (Fig. 6; Table S7). The first slope is close to the ratio of illite, 65 (Jeong and Achterberg, 2014) and the second slope is between the ratios of illite-smectite series clay minerals and chlorite, which are 128 and 464, respectively (Table S8). Kessler et al. (2020) also observed two-stage linear correlations of Fe, Al, and Si with DFB addition, with a strong linear correlation (Fe/Si slope of 54) in their later period (24–192 h) although their data did not show correlations in the early dissolution period (0–8 h). The concentrations of DFB-extractable Mn and Si also exhibited a strong linear correlation, with comparable slopes for the early and later periods to be 12 and 15 (r^2 = 0.75 and 0.88), respectively, which were significantly higher than the slope of 4.9, observed in the Control treatment for the later stage (after 24 h, $r^2 = 0.82$) (Fig. 6; Table S7). Co exhibited a two-stage correlation with Si during the 0–6 h period and after (Fig. 6), with slopes of 0.16 and 0.16 (r^2 = 0.81 and 0.94) for the early and late periods, compared to the slopes of 0.25 and 0.08 for the non-addition treatment (r^2 = 0.89 and 0.80), respectively. For Ni, the correlation was only significant after 12 h in the addition treatment ($r^2 = 0.84$), with a ratio of 0.86. Once again, the metal (Mn, Co, and Ni) ratios to Si and Al (Table S8 and S9) were comparable to the ratios of smectite reported by Bishop et al., 2002, suggesting that aluminosilicates are likely sources of these metals as well.

On the other hand, for Cd and Pb, as their dissolution at the initial time point (1 h) was already close to the maximum soluble concentrations observed during the entire 720 h period, their soluble concentrations did not significantly increase with increasing Si. For Zn, the correlation was observed for both addition and Control treatments during the early stage, with slopes of 23 and 13 from 0 to 24 h ($r^2 = 0.89$ and 0.88), which were approximately two orders of magnitude higher than lithogenic ratios, indicating that the extractable Zn originated from non-lithogenic materials. Similar to Cd and Pb, the dissolution of Zn relative to Si in the later stage became insignificant for both DFB addition and Control treatments (Fig. 6).

By comparing the dissolvable metal to Al ratios (M/Al) in different dissolution periods with the bulk ratios of f1, f5, and some specific lithogenic materials, including the upper crust and two common clay minerals, smectite and illite (Fig. S1, Hu and Gao, 2008; Bishop et al., 2002; Jeong and Achterberg, 2014), we observed that the initial dissolution ratios (0–1 h) of both f5 and f1 were either close to or higher than the bulk f1 ratios for most metals. Then the ratios generally decreased with time and approached the ratios of the lithogenic minerals (Fig. S1; Table S9). Except for Al and Fe, the average dissolved Al/Si and Fe/Si ratios in 1 h were 639 and 208, respectively, which were similar to the later periods. However, the dissolved M/Si ratios in 1 h for all other metals are much higher than the slopes observed in the later period (Fig. 6). With high enrichment factors (Fig. 3), extremely high dissolution rates in 1 h (Fig. 5), and high dissolved M/Si ratios in 1 h (Fig. 6), it is highly likely that anthropogenic aerosols were the dominant sources for most of the dissolvable metals in f5 within 1 h. Anthropogenic aerosols likely contributed to a significant fraction of the dissolvable Fe and Al in f5 within 1 h. Since anthropogenic aerosols are highly likely to be the major source of soluble metals in the 1 h period for both f1 and f5, we may estimate the lower limit of anthropogenic contribution in f5 from the dissolved metal concentrations in the 1 h. Moreover, with highly linear correlations with Si ($r^2 > 0.8$, $p < 0.05$) for some elements after 1 h and comparable M/Si ratios to some types of aluminosilicates, some of the extractable metals may originate from lithogenic minerals for later dissolution periods. The quantitative contribution of aluminosilicate-associated dissolved metal (dM_{Si}) to the total soluble concentrations may be estimated by multiplying dissolved silicate with the M/Si ratios (Table S7). The sum of the anthropogenic and lithogenic dissolvable metals estimated by these two independent approaches are relatively close to the measured value over 720 h (Table S10), strongly supporting our argument for the importance of different aerosol sources during different dissolution periods. Without DFB addition, anthropogenic aerosols accounted for at least 61 to 89% of the total soluble metals for most elements (except Fe and Al). With DFB addition, the contribution slightly decreased to levels ranging from 44 to 85% for the elements (Table S10). These results imply that the relative contribution of anthropogenic and lithogenic aerosols to the soluble metals appears to be element-specific and would be dependent on aerosol residence times in surface waters. With increasing aerosol residence time in the euphotic zone, the contribution of aerosol dissolvable metals from lithogenic sources would increase.

4. Conclusion

This study has characterized the dissolution kinetics of East Asian fine and coarse aerosol metals and tried to quantify the relative contribution of anthropogenic and lithogenic aerosols with dissolution time up to 30 days. Anthropogenic aerosols in both the finest and coarsest aerosols (f1 and f5) appear to be the major sources of instantaneously soluble aerosol metals within 1 h. On the other hand, lithogenic aerosols are the major source of slowly dissolvable aerosol metals, particularly in f5, which can gradually release soluble metals and can be further solubilized by the interaction with existing organic ligands over a relatively long time scale, at least lasting 30 days. Lithogenic aerosols thereby serve as a more sustainable source of soluble metals than anthropogenic aerosols for phytoplankton if aerosol particles remain suspended in the euphotic zone of the surface ocean long enough. We have also demonstrated the role of a model siderophore (DFB) on extracting Fe and some other biologically sensitive metals (e.g., Mn, Zn, Co, Ni, Cd) from lithogenic aerosols with time. It should be noted that DFB only accounts for a fraction of the total Fe binding ligands (1–2 nM) and our findings only reflect the effects of siderophore-like ligands. In conclusion, this study has demonstrated the relative roles of anthropogenic and lithogenic aerosols with dissolution time and the interaction of aerosol metals with the model organic ligand on influencing the supply of aerosol soluble metals in the surface ocean.

Data availability

Data will be made available on request.

Acknowledgments

We are deeply grateful to the two reviewers and Associate Editor William Landing for their invaluable comments, which have greatly enhanced the quality of this manuscript. We appreciate the technical assistance of H.-Y. Chen, K.-P. Chiang, and M.-C. Lu for aerosol sampling and silicate analysis in this study. We thank S.-C. Pai, L.-S. Wen, H.-T. Lin, and W.-H. Liao for their valuable comments and suggestions on this study. This study was financially supported by grants 108-2611-M-001-006-MY3 and 111-2611-M-001-006-MY3 from National Science and Technology Council, Taiwan and Investigator Award AS-IA-110-M03 by Academia Sinica to T.-Y. Ho.

Appendix A. Supplementary data

Supplementary data to this article can be found online at https://doi.org/10.1016/j.marchem.2023.104277.

References

Akafia, M.M., Harrington, J.M., Bargar, J.R., Duckworth, O.W., 2014. Metal oxyhydroxide dissolution as promoted by structurally diverse siderophores and oxalate. Geochim. Cosmochim. Acta 141, 258–269. https://doi.org/10.1016/j.gca.2014.06.024.

Baker, A.R., Li, M., Chance, R., 2020. Trace metal fractional solubility in size-segregated aerosols from the tropical eastern Atlantic Ocean. Glob. Biogeochem. Cycles 34 (6). https://doi.org/10.1029/2019GB006510 e2019GB006510.

Bi, Y., Hesterberg, D.L., Duckworth, O.W., 2010. Siderophore-promoted dissolution of cobalt from hydroxide minerals. Geochim. Cosmochim. Acta 74 (10), 2915–2925. https://doi.org/10.1016/j.gca.2010.02.028.

Bishop, J., Madejová, J., Komadel, P., Fröschl, H., 2002. The influence of structural Fe, Al and Mg on the infrared OH bands in spectra of dioctahedral smectites. Clay Miner. 37 (4), 607–616. https://doi.org/10.1180/0009855023740063.

Black, E., et al., 2020. Ironing out Fe residence time in the dynamic upper ocean. Glob. Biogeochem. Cycles 34 (9). https://doi.org/10.1029/2020GB006592 e2020GB006592.

Boiteau, R.M., et al., 2016. Siderophore-based microbial adaptations to iron scarcity across the eastern Pacific Ocean. Proc. Natl. Acad. Sci. U. S. A. 113 (50), 14237–14242. https://doi.org/10.1073/pnas.1608594113.

Borer, P.M., Sulzberger, B., Reichard, P., Kraemer, S.M., 2005. Effect of siderophores on the light-induced dissolution of colloidal iron (III)(hydr) oxides. Mar. Chem. 93 (2–4), 179–193. https://doi.org/10.1016/j.marchem.2004.08.006.

Bruland, K., Middag, R., Lohan, M., 2013. Controls of Trace Metals in Seawater. https://doi.org/10.1016/B978-0-08-095975-7.00602-1.

Bundy, R.M., et al., 2018. Distinct siderophores contribute to iron cycling in the mesopelagic at station ALOHA. Front. Mar. Sci. 5, 61. https://doi.org/10.3389/fmars.2018.00061.

Croot, P.L., Streu, P., Baker, A.R., 2004. Short residence time for iron in surface seawater impacted by atmospheric dry deposition from Saharan dust events. Geophys. Res. Lett. 31 (23) https://doi.org/10.1029/2004GL020153.

Dammshäuser, A., Wagener, T., Garbe-Schönberg, D., Croot, P., 2013. Particulate and dissolved aluminum and titanium in the upper water column of the Atlantic Ocean. Deep-Sea Res. I Oceanogr. Res. Pap. 73, 127–139. https://doi.org/10.1016/j.dsr.2012.12.002.

Datta, S., et al., 2012. Use of X-ray absorption spectroscopy to speciate manganese in airborne particulate matter from five counties across the United States. Environ. Sci. Technol. 46 (6), 3101–3109. https://doi.org/10.1021/es203435n.

Dauphas, N., et al., 2004. Chromatographic separation and multicollection-ICPMS analysis of iron. Investigating mass-dependent and -independent isotope effects. Anal. Chem. 76 (19), 5855–5863. https://doi.org/10.1021/ac0497095.

Desboeufs, K.V., Losno, R., Vimeux, F., Cholbi, S., 1999. The pH-dependent dissolution of wind-transported Saharan dust. J. Geophys. Res.-Atmos. 104 (D17), 21287–21299. https://doi.org/10.1029/1999JD900236.

Desboeufs, K.V., Sofikitis, A., Losno, R., Colin, J.L., Ausset, P., 2005. Dissolution and solubility of trace metals from natural and anthropogenic aerosol particulate matter. Chemosphere 58 (2), 195–203. https://doi.org/10.1016/j.chemosphere.2004.02.025.

Duce, R., et al., 1991. The atmospheric input of trace species to the world ocean. Glob. Biogeochem. Cycles 5 (3), 193–259. https://doi.org/10.1029/91GB01778.

Duckworth, O.W., et al., 2009. The exceptionally stable cobalt (III)–desferrioxamine B complex. Mar. Chem. 113 (1–2), 114–122. https://doi.org/10.1016/j.marchem.2009.01.003.

Ellwood, M.J., van den Berg, C.M., 2001. Determination of organic complexation of cobalt in seawater by cathodic stripping voltammetry. Mar. Chem. 75 (1–2), 33–47. https://doi.org/10.1016/S0304-4203(01)00024-X.

Fishwick, M.P., et al., 2014. The impact of changing surface ocean conditions on the dissolution of aerosol iron. Glob. Biogeochem. Cycles 28 (11), 1235–1250. https://doi.org/10.1002/2014gb004921.

Ho, T.-Y., Wen, L.-S., You, C.-F., Lee, D.-C., 2007. The trace metal composition of size-fractionated plankton in the South China Sea: biotic versus abiotic sources. Limnol. Oceanogr. 52 (5), 1776–1788. https://doi.org/10.4319/lo.2007.52.5.1776.

Ho, T.-Y., Chien, C.-T., Wang, B.-N., Siriraks, A., 2010a. Determination of trace metals in seawater by an automated flow injection ion chromatograph pretreatment system with ICPMS. Talanta 82, 1478–1484.

Ho, T.-Y., et al., 2010b. Trace metal cycling in the surface water of the South China Sea: vertical fluxes, composition, and sources. Limnol. Oceanogr. 55 (5), 1807–1820. https://doi.org/10.4319/lo.2010.55.5.1807.

Ho, T.-Y., Chou, W.-C., Lin, H.-L., Sheu, D.D., 2011. Trace metal cycling in the deep water of the South China Sea: the composition, sources, and fluxes of sinking particles. Limnol. Oceanogr. 56 (4), 1225–1243. https://doi.org/10.4319/lo.2011.56.4.1225.

Ho, T.-Y., You, C.-F., Chou, W.-C., Pai, S.-C., Wen, L.-S., Sheu, D.D., 2009. Cadmium and phosphorus cycling in the water column of the South China Sea: the roles of biotic and abiotic particles. Marine Chem. 115, 125–133. https://doi.org/10.1016/j.marchem.2009.07.005.

Hsieh, C.-C., Chen, H.-Y., Ho, T.-Y., 2022. The effect of aerosol size on Fe solubility and deposition flux: a case study in the East China Sea. Mar. Chem. 241, 104106 https://doi.org/10.1016/j.marchem.2022.104106.

Hsieh, C.-C., You, C.-F., Ho, T.-Y., 2023. The solubility and deposition flux of East Asian aerosol metals in the East China Sea: the effects of aeolian transport processes. https://doi.org/10.1016/j.marchem.2023.104268.

Hu, Z., Gao, S., 2008. Upper crustal abundances of trace elements: a revision and update. Chem. Geol. 253 (3–4), 205–221. https://doi.org/10.1016/j.chemgeo.2008.05.010.

Huggins, F.E., et al., 2011. Determination of nickel species in stack emissions from eight residual oil-fired utility steam-generating units. Environ. Sci. Technol. 45 (14), 6188–6195. https://doi.org/10.1021/es200823a.

Jeong, G.Y., 2008. Bulk and single-particle mineralogy of Asian dust and a comparison with its source soils. J. Geophys. Res.-Atmos. 113 (D2) https://doi.org/10.1029/2007JD008606.

Jeong, G., Achterberg, E.P., 2014. Chemistry and mineralogy of clay minerals in Asian and Saharan dusts and the implications for iron supply to the oceans. Atmos. Chem. Phys. 14 (22), 12415–12428. https://doi.org/10.5194/acp-14-12415-2014.

Jickells, T., et al., 2005. Global iron connections between desert dust, ocean biogeochemistry, and climate. Science 308 (5718), 67–71. https://doi.org/10.1126/science.1105959.

Kessler, N., Kraemer, S.M., Shaked, Y., Schenkeveld, W.D.C., 2020. Investigation of Siderophore-promoted and reductive dissolution of dust in marine microenvironments such as *Trichodesmium* colonies. Front. Mar. Sci. 7 https://doi.org/10.3389/fmars.2020.00045.

Kondo, Y., Bamba, R., Obata, H., Nishioka, J., Takeda, S., 2021. Distinct profiles of size-fractionated iron-binding ligands between the eastern and western subarctic Pacific. Sci. Rep. 11 (1), 1–9. https://doi.org/10.1038/s41598-021-81536-6.

Mackey, K.R., Chien, C.T., Post, A.F., Saito, M.A., Paytan, A., 2014. Rapid and gradual modes of aerosol trace metal dissolution in seawater. Front. Microbiol. 5, 794. https://doi.org/10.3389/fmicb.2014.00794.

Mahowald, N.M., et al., 2018. Aerosol trace metal leaching and impacts on marine microorganisms. Nat. Commun. 9 (1), 2614. https://doi.org/10.1038/s41467-018-04970-7.

Moore, L.E., Heller, M.I., Barbeau, K.A., Moffett, J.W., Bundy, R.M., 2021. Organic complexation of iron by strong ligands and siderophores in the eastern tropical North Pacific oxygen deficient zone. Mar. Chem. 236, 104021 https://doi.org/10.1016/j.marchem.2021.104021.

Morel, F.M.M., 2008. The co-evolution of phytoplankton and trace element cycles in the oceans. Geobiology 6 (3), 318–324. https://doi.org/10.1111/j.1472-4669.2008.00144.x.

Morel, F.M.M., Price, N.M., 2003. The biogeochemical cycles of trace metals in the oceans. Science 300 (5621), 944–947. https://doi.org/10.1126/science.1083545.

Ohnemus, D.C., et al., 2014. Laboratory intercomparison of marine particulate digestions including Piranha: a novel chemical method for dissolution of polyethersulfone filters. Limnol. Oceanogr. Methods 12 (8), 530–547. https://doi.org/10.4319/lom.2014.12.530.

Osán, J., et al., 2010. Speciation of copper and zinc in size-fractionated atmospheric particulate matter using total reflection mode X-ray absorption near-edge structure spectrometry. Spectrochim. Acta B At. Spectrosc. 65 (12), 1008–1013. https://doi.org/10.1016/j.sab.2010.11.002.

Park, J., et al., 2022. Siderophore production and utilization by microbes in the North Pacific Ocean. bioRxiv. https://doi.org/10.1101/2022.02.26.482025.

Pattanaik, S., Huggins, F.E., Huffman, G.P., 2012. Chemical speciation of Fe and Ni in residual oil fly ash fine particulate matter using X-ray absorption spectroscopy. Environ. Sci. Technol. 46 (23), 12927–12935. https://doi.org/10.1021/es301080s.

Ramachandran, R., Gupta, P., 1985. An improved spectrophotometric determination of silicate in water based on molybdenum blue. Anal. Chim. Acta 172, 307–311. https://doi.org/10.1016/S0003-2670(00)82621-5.

Saito, M.A., Goepfert, T.J., 2008. Zinc-cobalt colimitation of Phaeocystis antarctica. Limnol. Oceanogr. 53 (1), 266–275. https://doi.org/10.4319/lo.2008.53.1.0266.

Sakata, K., et al., 2014. Identification of sources of lead in the atmosphere by chemical speciation using X-ray absorption near-edge structure (XANES) spectroscopy. J. Environ. Sci. (China) 26 (2), 343–352. https://doi.org/10.1016/s1001-0742(13)60430-1.

Sakata, K., Sakaguchi, A., Yokoyama, Y., Terada, Y., Takahashi, Y., 2017. Lead speciation studies on coarse and fine aerosol particles by bulk and micro X-ray absorption fine structure spectroscopy. Geochem. J. 51 (3), 215–225. https://doi.org/10.2343/geochemj.2.0456.

Schijf, J., Christenson, E.A., Potter, K.J., 2015. Different binding modes of Cu and Pb vs. Cd, Ni, and Zn with the trihydroxamate siderophore desferrioxamine B at seawater ionic strength. Mar. Chem. 173, 40–51. https://doi.org/10.1016/j.marchem.2015.02.014.

Shao, L., Li, W., Yang, S., Shi, Z., Lü, S., 2007. Mineralogical characteristics of airborne particles collected in Beijing during a severe Asian dust storm period in spring 2002. Sci. China Ser. D Earth Sci. 50 (6), 953–959. https://doi.org/10.1007/s11430-007-0035-7.

Sohrin, Y., et al., 2008. Multielemental determination of GEOTRACES key trace metals in seawater by ICPMS after preconcentration using an ethylenediaminetriacetic acid chelating resin. Anal. Chem. 80 (16), 6267–6273. https://doi.org/10.1021/ac800500f.

Thuróczy, C.-E., Boye, M., Losno, R., 2010. Dissolution of cobalt and zinc from natural and anthropogenic dusts in seawater. Biogeosciences 7 (6), 1927–1936. https://doi.org/10.5194/bg-7-1927-2010.

Wang, B.-S., Ho, T.-Y., 2020. Aerosol Fe cycling in the surface water of the Northwestern Pacific Ocean. Prog. Oceanogr. 183, 102291 https://doi.org/10.1016/j.pocean.2020.102291.

Wang, B.-S., Lee, C.-P., Ho, T.-Y., 2014. Trace metal determination in natural waters by automated solid phase extraction system and ICP-MS: the influence of low level Mg and Ca. Talanta 128, 337–344. https://doi.org/10.1016/j.talanta.2014.04.077.

Wang, J., Zhang, J., Liu, X., Liu, B., Yao, X., Gao, H., 2023. Atmospheric input of silicon to the China adjacent seas: non-negligible contributions from anthropogenic sources. Sci. Total Environ. https://doi.org/10.1016/j.scitotenv.2022.159540.